Hindawi Publishing Corporation
Journal of Nanomaterials
Volume 2014, Article ID 175670, 7 pages
http://dx.doi.org/10.1155/2014/175670

Research Article

Fabrication of Gold Nanodot Array for the Localized Surface Plasmon Resonance

Young Min Bae, Kyeong-Hee Lee, Jeongwon Yang, and Duchang Heo

Korea Electrotechnology Research Institute, 111 Hanggaul-ro, Ansan 426-170, Republic of Korea

Correspondence should be addressed to Young Min Bae; kimbym@keri.re.kr

Received 23 July 2014; Revised 24 September 2014; Accepted 25 September 2014; Published 13 October 2014

Academic Editor: Chunyi Zhi

Localized surface plasmon resonance (LSPR) is a promising method for detecting antigen-antibody binding in label-free biosensors. In this study, the fabrication of a LSPR substrate with a gold nanodot array through the lift-off process of an alumina mask is reported. The substrate showed an extinction peak in its extinction spectrum, and the peak position was dependent on the height of the gold nanodot array, and the change of extinction peak with the height could be predicted by the numerical simulation. In addition, the peak position was observed to be red-shifted with the increasing RIU value of the medium surrounding the gold nanodot array. In particular, the peak position in the 10 nm thick gold nanodot array was approximately 710 nm in air, and the sensitivity, defined as the ratio of the shift of peak position to the RIU of the medium, was 323.6 nm/RIU. The fabrication procedure could be applied to fabricate the LSPR substrates with a large area.

1. Introduction

When light is incident on a surface with metal nanoparticles smaller than the wavelength of light, the collective oscillation of conduction electron in them with a resonant frequency is induced [1]. As the metal nanoparticles absorb and scatter the light in the localized surface plasmon resonance (LSPR) mode, the resonance frequency can be estimated via measuring the light transmittance of nanoparticles. This resonance frequency depends on the nanoparticles' size, shape, composition, and a local dielectric medium surrounding them. The refractive index change of local dielectric medium due to absorbing organic molecules onto the nanoparticles results in the change of resonance frequency. Therefore, LSPR provides a methodology for label-free detection in biosensor technology such as immunoassay and detection or monitoring of DNA hybridization [2–4].

The substrate, onto which the nanosized metal structures exhibiting the LSPR phenomenon are deposited, should be developed for the LSPR-based biosensor. There have been several methods reported to fabricate the substrate for LSPR, such as the direct deposition of nanoparticles or nanorods in solution onto a solid surface, the growth of nanoparticles on the surface, nanosphere lithography, and nanoimprint lithography [5–12]. The nanosphere lithography was used to systematically investigate the effect of nanoparticle size and shape on LSPR results [7, 8]. However, it is not easy to fabricate the packed nanosphere array over a substrate with a large area, even though several other fabrication protocols have been proposed [13]. On the other hand, an alumina film with nanopores, which was prepared by anodizing aluminum foil in an acidic solution, has been used to fabricate nanostructures [14]. The pores are highly ordered over the entire alumina film, and the size and density of the pores are controlled by changing the anodization conditions such as the acid pH value and applied voltage [15–17]. Devices or surfaces such as a carbon nanotube emitter, silicon nanodot array, superhydrophobic surface, and optical filter were prepared using the alumina films [18–21]. According to these examples, the anodization process is advantageous in that it confines the structure to the nanoscale and is fully controllable. Moreover, as alumina films with a large surface area can be prepared by anodizing the aluminum foil, the fabrication of an LSPR substrate using an alumina mask is a potential candidate for developing an LSPR-based biosensor [22, 23]. However, as the alumina mask is fabricated with a thick aluminum foil

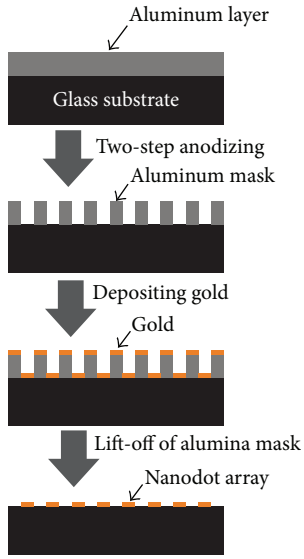

Figure 1: Fabrication of the gold nanodot array on substrate using the alumina mask lift-off process.

followed by transferring it onto the substrate, it is difficult to handle it due to the several hundred nanometer thickness [24, 25].

In this study, the fabrication of a gold nanodot array using the alumina mask is reported for the LSPR substrate. It is unique that the alumina mask was prepared by anodizing the aluminum film deposited on the substrate, so, it does not need to handle the thin alumina mask. A glass substrate was used as the substrate in order to observe the LSPR phenomenon by measuring transmittance of the substrate, and the LSPR phenomenon was compared to the numerical estimation. Finally, the applicability of it to the LSPR-based biosensor was investigated.

2. Methods

2.1. Fabrication of Gold Nanodot Array. Fabrication of the gold nanodot array on glass substrate is schematically illustrated in Figure 1. After a glass substrate (size: 24 × 24 mm) was cleaned with the piranha solution (1 : 4 of hydrogel peroxide and sulfuric acid), 1 μm thick aluminum film was deposited by electron beam evaporation (EI-5, ULVAC Co., USA). A two-step anodization process was executed to form the alumina mask on the substrate as described elsewhere [15]. Figure 2(a) shows the experimental setup for the anodization process. The change in the electric current between the substrate and the carbon electrode was recorded during each anodization using the bench top multimeter (34401A, Agilent Co., USA). In the first anodization process, after the substrate and the carbon electrode were placed in a beaker of 0.3 M oxalic acid, 40 V was applied between the substrate and the carbon electrode to anodize the aluminum film for 13 minutes at 5°C. The alumina film formed on the substrate was removed by immersing it in a solution of 6 wt% H_3PO_4 and 1.5 wt% CrO_3 at 60°C. After the substrate was rinsed and dried, the second anodization process was executed with the aluminum film remaining on the substrate under the same conditions as the first anodization. Finally, the substrate was immersed in a beaker of 5 wt% H_3PO_4 to remove the barrier layer and widen the diameter of the pores formed in the alumina film.

The gold nanodot array was fabricated using the alumina mask lift-off process. To fabricate the gold nanodot array, a 2 nm thick layer of chromium and a gold layer were sequentially deposited via electron beam evaporation onto the substrate. After depositing the gold layer, the alumina mask was removed by immersing the substrate in 5 wt% H_3PO_4 at 30°C for 60 minutes.

2.2. Characterization of Gold Nanodot Arrays. Scanning electron micrographs (SEM) of the alumina mask and the gold nanodot arrays were acquired using field emission scanning electron microscopy (S-4800, Hitachi Co., Japan), and the size of gold nanodot was estimated from the SEM with the imaging processing software embedded in the instrument. The extinction spectra of the gold nanodot arrays were estimated as the logarithmic value of the reciprocal of transmittance measured using a spectrophotometer (Evolution 300, Thermo Scientific Co.) with a resolution of 1 nm. The spectrophotometer is operated in the dual-beam mode and has a xenon lamp and a silicon photodiodes as a light source and detector. In addition, the extinction spectra of the gold nanodot arrays with the surrounding medium were estimated by measuring the spectra by immersing the substrate in the glass cuvette in which the water or the mixture of water and glycerol was contained.

3. Results and Discussion

The gold nanodot array on glass substrate was fabricated with the lift-off process of the alumina mask shown as schematically illustrated in Figure 1. The alumina mask was prepared using a two-step anodization process. In this study, the two-step anodization process was executed with a 1 μm thick aluminum film deposited onto a glass substrate to make the thin alumina mask attached to the substrate. In the first anodization step, a portion of aluminum film was anodized, and the alumina film formed on the aluminum film was removed. In the second anodization step, the remaining aluminum film was converted to the alumina film via complete anodization. The alumina mask was completed by removing the barrier layer existing at the bottom of the nanopores in the alumina film and widening the pore size.

The change in electric current as a function of the anodization time was recorded during the first and second anodization steps (Figure 2(b)). Additionally, the one-step anodization of the aluminum layer on the glass was recorded under the same conditions. It took approximately 19 minutes for the current to drop in the one-step anodization process. In the two-step anodization process, the first anodization step was carried out for 13 minutes. The current increased slightly with time but only after experiencing an initial drop. In the second anodization step, the current began to decrease after

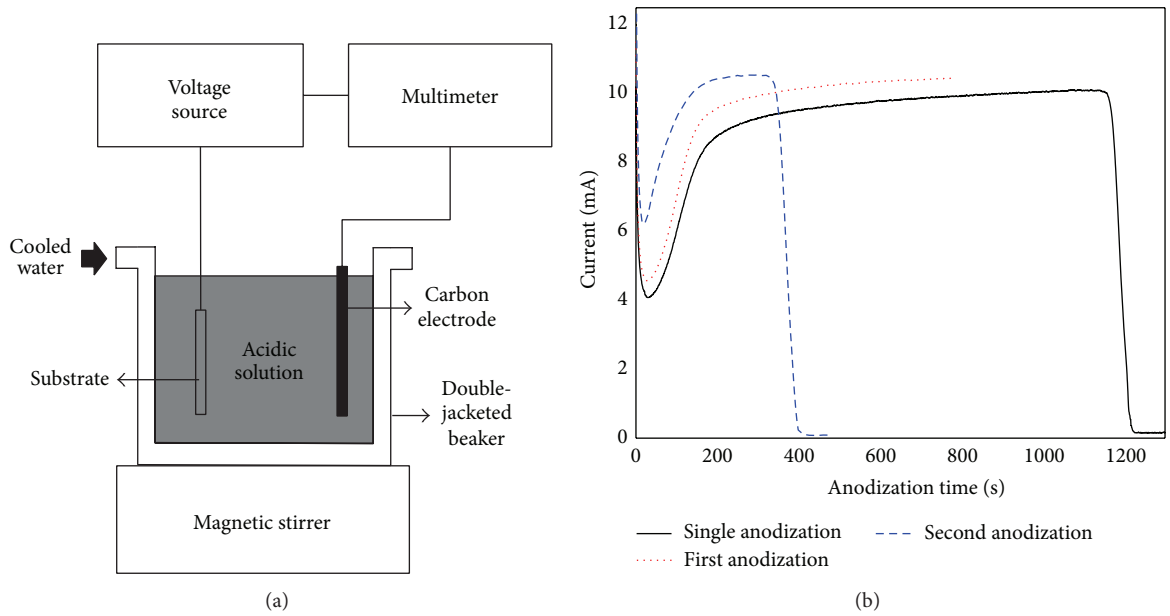

FIGURE 2: (a) Experimental setup for anodizing the aluminum film on the substrate. (b) Change in current as a function of anodization time in the single-step and two-step anodization processes.

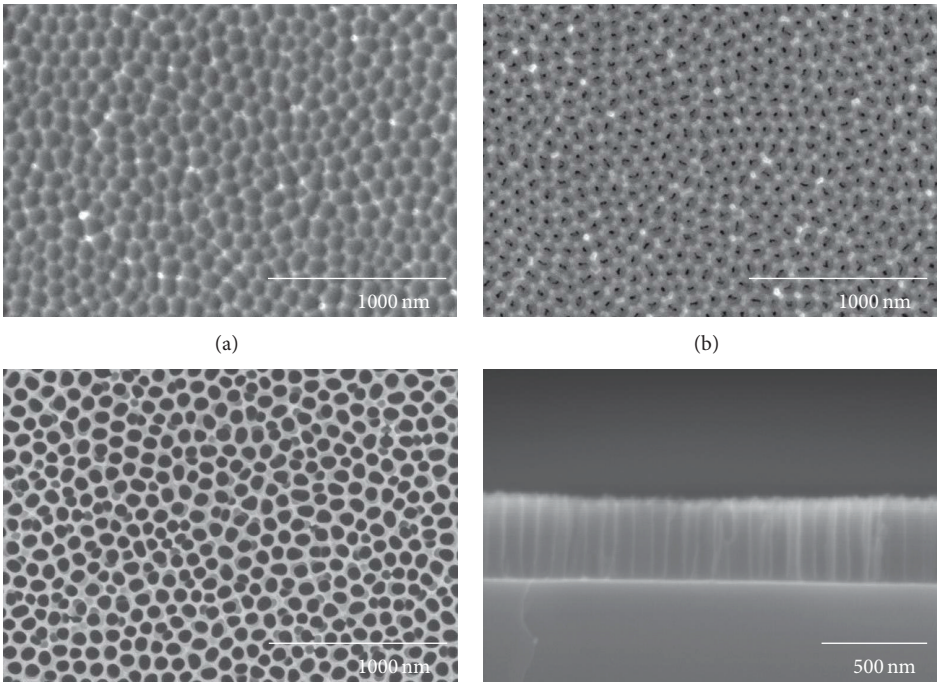

FIGURE 3: Scanning electron micrographs of alumina film on glass substrate. (a) The surface of aluminum layer after the first anodization. (b) The surface of alumina film after the second anodization. (c) The surface of alumina mask completed after removing the barrier layer. (d) The cross-sectional view of the alumina mask.

approximately 5.5 minutes as the aluminum layer became semitransparent, which indicated that the aluminum layer was fully converted into an alumina film. After the current dropped, the anodization process was continued for more than 1 minute to confirm that the aluminum layer was completely anodized. The total aluminum anodization time for the two-step anodization process was approximately 18.5 minutes, which was nearly equal to the amount of time as the one-step anodization process.

Figure 3(a) shows the surface morphology of the aluminum film on the substrate which was acquired using field emission scanning electron microscopy after the first

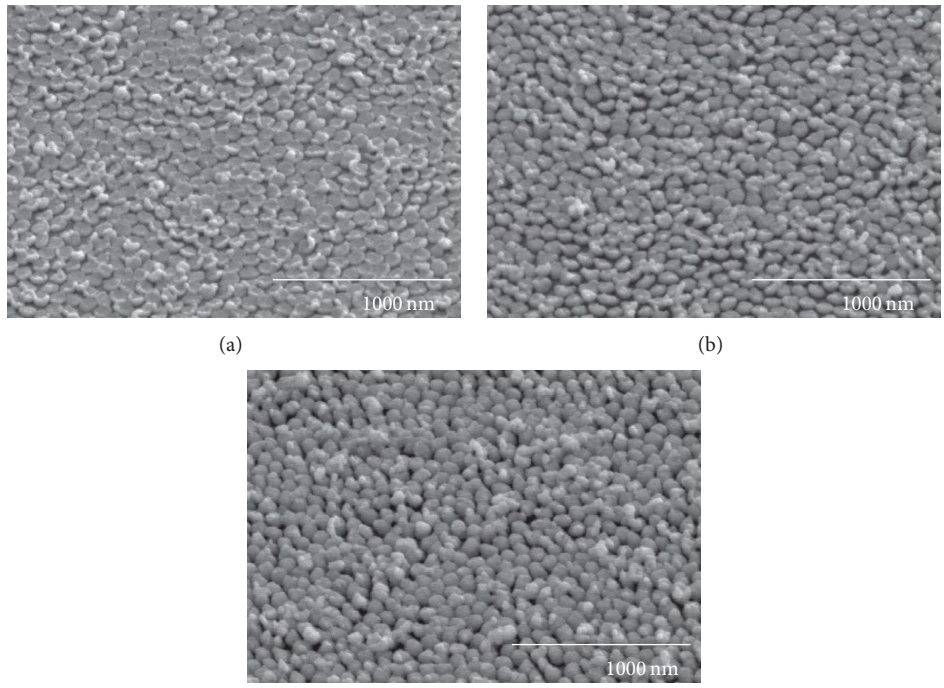

(a) (b)

(c)

Figure 4: Scanning electron micrographs of the (a) 10, (b) 30, and (c) 50 nm thick gold nanodot arrays formed on glass substrate. All the micrographs were acquired from the sample tilted with 45°.

anodization step followed by the removal of alumina. The mesh pattern was observed on the surface after the first anodization step [22]. After the second anodization step, the nanosized pores were formed on the alumina film as shown in Figure 3(b). As the barrier layer is formed at the bottom of pores of the alumina films, it should be removed so that the alumina film can be used as the lift-off mask [14]. As the barrier layer is of aluminum oxide, it can be resolved in the acidic solution such as the phosphoric acid [26, 27]. In this study, the alumina film on the substrate was wet-etched in a 5 wt% H_3PO_4 solution. Figures 3(c) and 3(d) show the surface of the alumina mask completed. The pores of the alumina mask in Figure 3(c) were larger than the pores shown in Figure 3(b). In the cross-sectional view of the alumina mask in Figure 3(d), it was observed that the pores were the through-hole type by removing the barrier layer in the bottom of pores. Although there have been several methods to remove the barrier layer such as the reactive ion etching or wet-etching, the barrier layer was simply removed during the etching [19, 26]. On the other hand, the thickness of the alumina mask was estimated to be approximately 390 nm in Figure 3(d). As the alumina film prepared in the first anodization step was removed, the remaining aluminum film was converted into an alumina mask in the second anodization step, and the thickness of mask is proportional to the second anodization time. By considering that the converted alumina film was 1.2 times thicker than the aluminum film, the thickness of alumina mask was calculated as 356.8 nm by multiplying the total converted alumina film (1.2 μm) by the ratio of the second anodization time (5.5 minutes) to the total anodization time (~18.5 minutes). The calculated value of the mask thickness was similar to the mask thickness estimated by the SEM analysis with an error of approximately 8.5%. It is important to control the thickness of the alumina mask, as the impending success or failure in the lift-off process is dictated by the thickness of the mask. For example, the substrate lift-off process failed when the first anodization step time exceeded more than 15 minutes in preliminary experiments.

A 2 nm thick chromium film serving as an adhesion layer, onto which a gold layer was later deposited, was deposited by electron beam evaporation onto the alumina masked substrate. The gold nanodot array on the substrate was completed using the alumina mask lift-off process, which consisted of immersing the substrate in a solution of 5 wt% H_3PO_4 at 30°C while stirring gently for 60 minutes. Figures 4(a)–4(c) show the gold nanodot array on the substrate according to the thickness of the gold layer deposited: 10, 30, and 50 nm, respectively. The lift-off process failed for the substrate with the gold layer thicker than 50 nm. The diameter of each gold nanodot was 93.3 ± 6.7 nm, 92.1 ± 6.4 nm, and 88.8 ± 5.6 nm for the gold layers measuring 10, 30, and 50 nm thick, respectively. Additionally, the center-to-center distance between each gold nanodot was 101 ± 7.5, 100 ± 8.7, and 97.5 ± 6.2 nm for the gold layers measuring 10, 30, and 50 nm thick, respectively.

Figure 5(a) shows the extinction spectra of the substrate with varying gold layer thickness. Each spectrum was measured while the surface of substrate exposed to air. The spectrum of the substrate with the 10 nm thick gold layer was broader than the other spectrums, but the peak position from

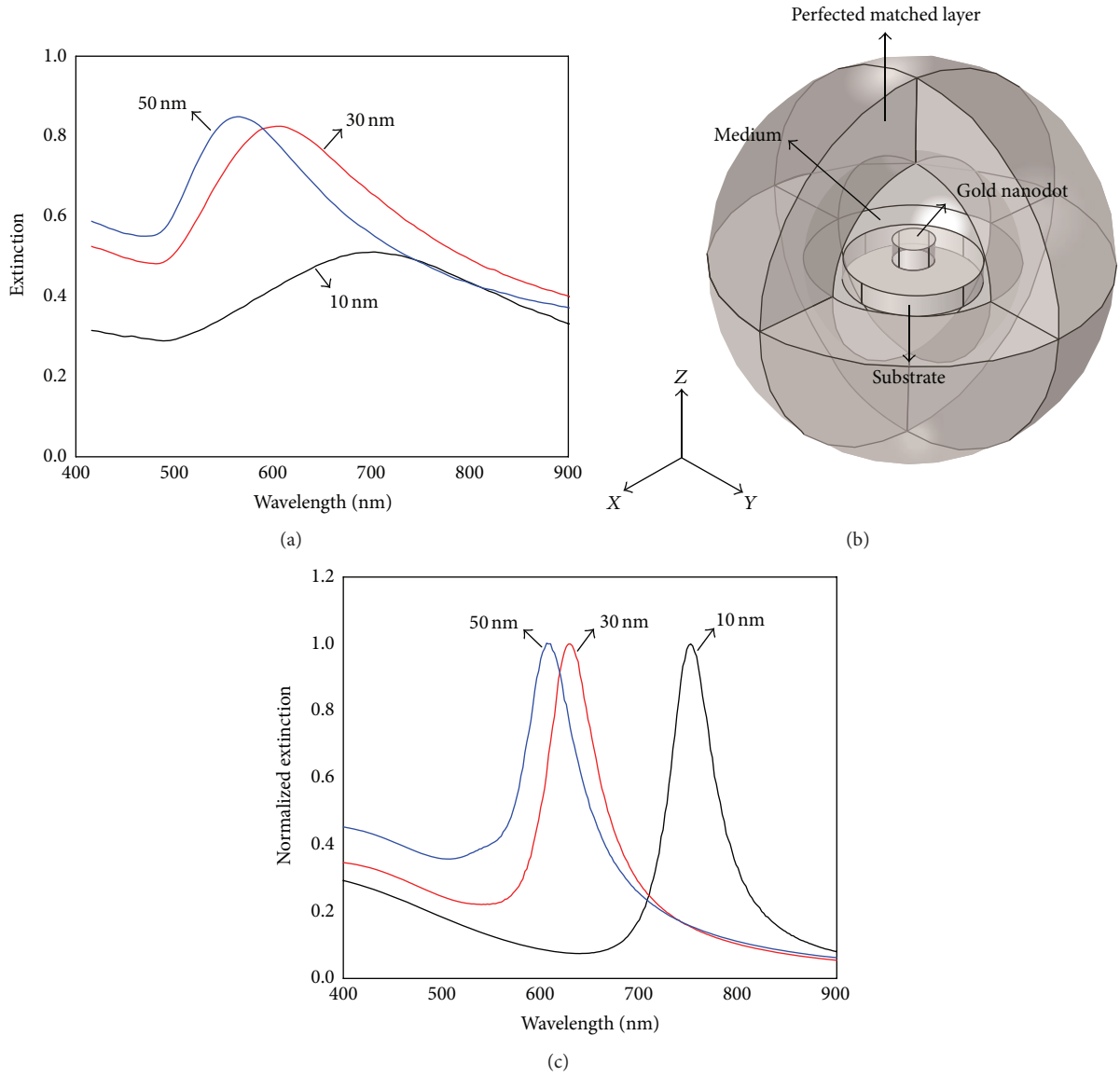

FIGURE 5: (a) Measured extinction spectrum of the substrate with the gold nanodot array formed by depositing various gold layer thicknesses. (b) The geometry model used for simulating the extinction spectrum of gold nanodot. (c) Simulated extinction spectrum of the substrate with the gold nanodot on the glass substrate.

the spectrum could be estimated with the centroid algorithm [28]. The peak position wavelength for the substrate with the 10 nm thick gold layer was 710 ± 11 nm, which was in the near-infrared range. Moreover, the peak positions for the substrate with the 30 and 50 nm thick gold layers were 606 ± 2 and 562 ±3 nm, respectively. When the light at a specific wavelength irradiates the metal nanoparticles, the collective oscillation of the conduction electron plasma localized within the near surface region of the nanoparticle occurs. This is the phenomenon for which LSPR is known and can be observed by the peak positions in the spectrum measured using extinction spectroscopy [8].

The extinction of gold nanodot array could be modeled using a finite element analysis (FEM) software package (COMSOL Multiphysics, USA) [29]. As shown in Figure 5(b), it was assumed that the gold nanodot on a glass substrate (the refractive index = 1.52) was cylindrical with the diameter estimated in the SEM analysis, and the medium surrounding the gold dot was air (the refractive index = 1), and the boundary condition of the medium was selected as the perfect matched layer (PML) function provided in the software package. The data reported in Johnson and Christy's article was used for the optical properties of gold [30]. The extinction cross section as the sum of absorption and scattering cross section was calculated with the FEM analysis under the condition that the electromagnetic field polarized in the x-axis was irradiated in the direction of z-axis in the geometry shown in Figure 5(b). Figure 5(c) shows the extinction spectra simulated in the different height of

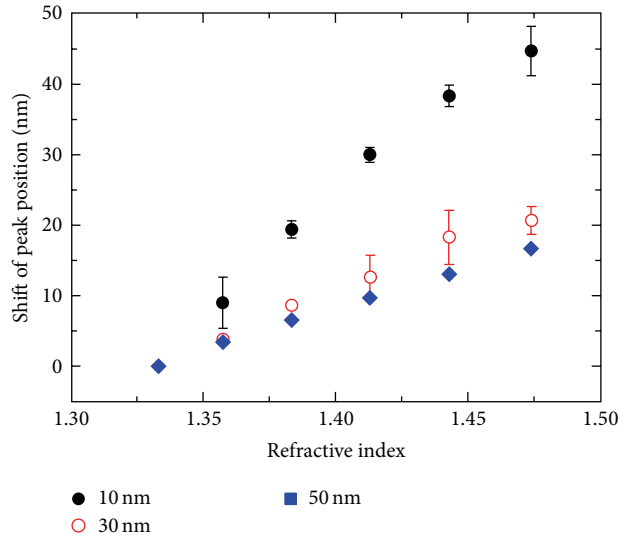

FIGURE 6: Measured data of shift in peak position of the extinction spectra of the gold nanodot arrays with 10, 30, and 50 nm thick gold deposition as a function of the refractive index of the medium.

10, 30, and 50 nm. The normalized extinction of the y-axis was calculated by dividing by the value in the peak of spectrum. The peak positions of gold nanodot array with 10, 30, and 50 nm heights were estimated to be, respectively, 752, 630, and 608 nm, which were higher than the values measured in the experiment. This difference between the experiment and the simulation is possibly due to a thin oxide layer on the surface of gold nanodot [31]. As the LSPR is sensitive to the refractive index of medium surrounding the metal, the LSPR of gold nanodot array in the experiment was affected by the oxide layer which prevented the surface of gold nanodot from being exposed to air. In addition, the disagreement of shapes of nanodot in both the experiment and the simulation could contribute to the difference of LSPR because the peak position of the extinction spectrum is affected by the size, shape, and composition of the nanoparticle. However, the trend of peak position with the varying height of gold nanodot coincided in both the experiment and the simulation. A similar change in peak position with increasing nanoparticle height has also been reported for substrates coated with Ag nanoparticles fabricated using nanosphere lithography [8].

The effects of the medium on the extinction spectrum of the nanodot array were also estimated by measuring the extinction spectra of gold nanodot array immersed in water-glycerol mixture. The RIU of the medium was adjusted with various concentrations of glycerol in water: 0 (pure water), 20, 40, 60, 80, and 100 (glycerol) wt%, which corresponded to RIU values of 1.3303, 1.35749, 1.383413, 1.41299, 1.4429, and 1.4739, respectively, at 20°C. When the medium was changed to the pure water in place of air, the spectrum peak position of the substrate with the 10, 30, and 50 nm thick gold layer was 785 ± 3, 642 ± 8, and 592 ± 1 nm, respectively; all of the peaks for the varying gold layer thickness shifted from the peak position measured in the air environment due to the change in the refractive index unit (RIU) of the surrounding medium. The shift in peak position relative to the peak position in the pure water as a function of the RIU of the surrounding medium is shown in Figure 6. From these results, it is clear that the peak position increased with the increasing RIU value of the medium. The equation reported by Kelly et al. indicates that the peak position is linearly proportional to the RIU value of the surrounding medium [5]. In the conducted experiment, the peak position was linearly shifted against the RIU value. The slope in Figure 6, which is calculated as the ratio of the peak position shift to the change of the surrounding medium RIU value, was 323.6, 150.9, and 116.3 nm/RIU for the substrate with the 10, 30, and 50 nm thick gold layer, respectively. In LSPR-based biosensing, the aforementioned slope is related to the sensitivity, and a tiny change in the RIU due to the antigen-antibody binding occurring on the substrate is converted to a readable signal. In view of the sensitivity, the LSPR substrate reported here is superior to the substrate fabricated using nanosphere lithography and provides sensitivity similar to the substrate fabricated using nanoimprint lithography [8, 12].

4. Conclusions

The gold nanodot array reported in this study successfully demonstrated the possibility to serve as an LSPR-based biosensor substrate. The peak position in the extinction spectrum was dependent on the height of the gold nanodot. In particular, the peak position in the extinction spectrum of the reported LSPR substrate with the 10 nm thick gold layer was in the near-infrared range. As the extinction bands of tissues or blood mainly exist at wavelengths lower than 650 nm, the LSPR substrate with the extinction peak in the near-infrared range reduces the noise interference due to tissue or blood complications. In view of the sensitivity, the ratio of the peak position shift to the surrounding medium RIU value was superior or comparable to the other types of substrates commonly used.

The substrate fabrication method used an alumina mask prepared through a two-step anodization process, which is a well-defined process used to construct nanosized structures over large areas. Although the substrate used in this study was limited to 24 × 24 mm, the size of the substrate can be increased by simply modifying the protocol. In conclusion, the reported methodology based on the anodization process can provide a simple and cost-effective method to fabricate LSPR substrates.

Conflict of Interests

The authors declare that there is no conflict of interests regarding the publication of this paper.

Acknowledgments

This research was supported by Korea Electrotechnology Research Institute (KERI) Primary Research Program

through the Korea Research Council for Industrial Science & Technology (ISTK) funded by the Ministry of Science, ICT and Future Planning (MSIP) (no. 14-12-N0101-05).

References

[1] M. E. Stewart, C. R. Anderton, L. B. Thompson et al., "Nanostructured plasmonic sensors," *Chemical Reviews*, vol. 108, no. 2, pp. 494–521, 2008.

[2] M. D. Zordan, M. M. G. Grafton, G. Acharya et al., "Detection of pathogenic E. coli O157:H7 by a hybrid microfluidic SPR and molecular imaging cytometry device," *Cytometry A*, vol. 75, no. 2, pp. 155–162, 2009.

[3] L. Guo and D.-H. Kim, "LSPR biomolecular assay with high sensitivity induced by aptamer-antigen-antibody sandwich complex," *Biosensors and Bioelectronics*, vol. 31, no. 1, pp. 567–570, 2012.

[4] K. A. Willets and R. P. van Duyne, "Localized surface plasmon resonance spectroscopy and sensing," *Annual Review of Physical Chemistry*, vol. 58, pp. 267–297, 2007.

[5] K. L. Kelly, E. Coronado, L. L. Zhao, and G. C. Schatz, "The optical properties of metal nanoparticles: the influence of size, shape, and dielectric environment," *Journal of Physical Chemistry B*, vol. 107, no. 3, pp. 668–677, 2003.

[6] D. A. Gish, F. Nsiah, M. T. McDermott, and M. J. Brett, "Localized surface plasmon resonance biosensor using silver nanostructures fabricated by glancing angle deposition," *Analytical Chemistry*, vol. 79, no. 11, pp. 4228–4232, 2007.

[7] J. N. Anker, W. P. Hall, O. Lyandres, N. C. Shah, J. Zhao, and R. P. van Duyne, "Biosensing with plasmonic nanosensors," *Nature Materials*, vol. 7, no. 6, pp. 442–453, 2008.

[8] C. L. Haynes and R. P. van Duyne, "Nanosphere lithography: a versatile nanofabrication tool for studies of size-dependent nanoparticle optics," *Journal of Physical Chemistry B*, vol. 105, no. 24, pp. 5599–5611, 2001.

[9] K. Mitsui, Y. Handa, and K. Kajikawa, "Optical fiber affinity biosensor based on localized surface plasmon resonance," *Applied Physics Letters*, vol. 85, no. 18, pp. 4231–4233, 2004.

[10] H. Huang, S. Huang, X. Liu et al., "Label-free optical biosensors based on Au2S-coated gold nanorods," *Biosensors and Bioelectronics*, vol. 24, no. 10, pp. 3025–3029, 2009.

[11] R. Gupta, M. J. Dyer, and W. A. Weimer, "Preparation and characterization of surface plasmon resonance tunable gold and silver films," *Journal of Applied Physics*, vol. 92, no. 9, pp. 5264–5271, 2002.

[12] S.-W. Lee, K.-S. Lee, J. Ahn, J.-J. Lee, M.-G. Kim, and Y.-B. Shin, "Highly sensitive biosensing using arrays of plasmonic Au nanodisks realized by nanoimprint lithography," *ACS Nano*, vol. 5, no. 2, pp. 897–904, 2011.

[13] R. Micheletto, H. Fukuda, and M. Ohtsu, "A simple method for the production of a two-dimensional, ordered array of small latex particles," *Langmuir*, vol. 11, no. 9, pp. 3333–3336, 1995.

[14] R. C. Furneaux, W. R. Rigby, and A. P. Davidson, "The formation of controlled-porosity membranes from anodically oxidized aluminium," *Nature*, vol. 337, no. 6203, pp. 147–149, 1989.

[15] H. Masuda and K. Fukuda, "Ordered metal nanohole arrays made by a two-step replication of honeycomb structures of anodic alumina," *Science*, vol. 268, no. 5216, pp. 1466–1468, 1995.

[16] K. Nielsch, J. Choi, K. Schwirn, R. B. Wehrspohn, and U. Gösele, "Self-ordering regimes of porous alumina: the 10 porosity rule," *Nano Letters*, vol. 2, no. 7, pp. 677–680, 2002.

[17] C. K. Chung, M. W. Liao, H. C. Chang, and C. T. Lee, "Effects of temperature and voltage mode on nanoporous anodic aluminum oxide films by one-step anodization," *Thin Solid Films*, vol. 520, no. 5, pp. 1554–1558, 2011.

[18] S.-K. Hwang, J. Lee, S.-H. Jeong, P.-S. Lee, and K.-H. Lee, "Fabrication of carbon nanotube emitters in an anodic aluminium oxide nanotemplate on a Si wafer by multi-step anodization," *Nanotechnology*, vol. 16, no. 6, pp. 850–858, 2005.

[19] B. Yan, H. T. M. Pham, Y. Ma, Y. Zhuang, and P. M. Sarro, "Fabrication of in situ ultrathin anodic aluminum oxide layers for nanostructuring on silicon substrate," *Applied Physics Letters*, vol. 91, no. 5, Article ID 053117, 2007.

[20] W. Lee, B. G. Park, D. H. Kim et al., "Nanostructure-dependent water-droplet adhesiveness change in superhydrophobic anodic aluminum oxide surfaces: from highly adhesive to self-cleanable," *Langmuir*, vol. 26, no. 3, pp. 1412–1415, 2010.

[21] Y. Zhang, S. J. Son, and H. Ju, "Anodized aluminum oxide membranes of tunable porosity with platinum nanoscale-coating for photonic application," *Current Applied Physics*, vol. 12, no. 6, pp. 1561–1565, 2012.

[22] D. Choi, Y. Choi, S. Hong, T. Kang, and L. P. Lee, "Self-organized hexagonal-nanopore SERS array," *Small*, vol. 6, no. 16, pp. 1741–1744, 2010.

[23] S.-H. Yeom, M.-E. Han, B.-H. Kang et al., "Enhancement of the sensitivity of LSPR-based CRP immunosensors by Au nanoparticle antibody conjugation," *Sensors and Actuators B: Chemical*, vol. 177, pp. 376–383, 2013.

[24] L. Nataraj and S. G. Cloutier, "Highly ordered periodic array of metallic nanodots fabricated through template-assisted nanopatterning and its use for surface-enhanced Raman scattering spectroscopy of flexible crystalline-silicon nanomembranes," *Journal of Raman Spectroscopy*, vol. 42, no. 6, pp. 1294–1297, 2011.

[25] Y. Lei, S. Yang, M. Wu, and G. Wilde, "Surface patterning using templates: concept, properties and device applications," *Chemical Society Reviews*, vol. 40, no. 3, pp. 1247–1258, 2011.

[26] M. S. Sander and L. S. Tan, "Nanoparticle arrays on surfaces fabricated using anodic alumina films as templates," *Advanced Functional Materials*, vol. 13, no. 5, pp. 393–397, 2003.

[27] H. Masuda, K. Yasui, Y. Sakamoto, M. Nakao, T. Tamamura, and K. Nishio, "Ideally ordered anodic porous alumina mask prepared by imprinting of vacuum-evaporated Al on Si," *Japanese Journal of Applied Physics, Part 2: Letters*, vol. 40, no. 11 B, pp. L1267–L1269, 2001.

[28] S. Zhan, X. Wang, and Y. Liu, "Fast centroid algorithm for determining the surface plasmon resonance angle using the fixed-boundary method," *Measurement Science and Technology*, vol. 22, no. 2, Article ID 025201, 2011.

[29] Z. Liu, A. Boltasseva, R. H. Pedersen et al., "Plasmonic nanoantenna arrays for the visible," *Metamaterials*, vol. 2, no. 1, pp. 45–51, 2008.

[30] P. B. Johnson and R. W. Christy, "Optical constants of the noble metals," *Physical Review B*, vol. 6, no. 12, pp. 4370–4379, 1972.

[31] M. D. Malinsky, K. Lance Kelly, G. C. Schatz, and R. P. van Duyne, "Nanosphere lithography: effect of substrate on the localized surface plasmon resonance spectrum of silver nanoparticles," *Journal of Physical Chemistry B*, vol. 105, no. 12, pp. 2343–2350, 2001.